Eur. Phys. J. B (2020) 93: 49
https://doi.org/10.1140/epjb/e2019-100514-8

THE EUROPEAN PHYSICAL JOURNAL B

Regular Article

Probabilistic motional averaging*

Denys S. Karpov[1,2,a], Vladimir Y. Monarkha[3,4], Daniel Szombati[3], Alejandro G. Frieiro[3,5], Aleksander N. Omelyanchouk[1], Evgeni Il'ichev[2,6], Arkady Fedorov[3], and Sergey N. Shevchenko[1,7]

[1] B. Verkin Institute for Low Temperature Physics and Engineering, Kharkov, Ukraine
[2] Leibniz Institute of Photonic Technology, Jena, Germany
[3] ARC Centre of Excellence for Engineered Quantum Systems, St. Lucia, Queensland 4072, Australia
[4] Okinawa Institute of Science and Technology Graduate University, Onna, 904-0495 Okinawa, Japan
[5] School of Mathematics and Physics, University of Queensland, St Lucia, Queensland 4072, Australia
[6] Novosibirsk State Technical University, Novosibirsk, Russia
[7] V. N. Karazin Kharkov National University, Kharkov, Ukraine

Received 22 October 2019 / Received in final form 3 December 2019
Published online 11 March 2020

Abstract. In a continuous measurement scheme a spin-1/2 particle can be measured and simultaneously driven by an external resonant signal. When the driving is weak, it does not prevent the particle wavefunction from collapsing and a detector randomly outputs two responses corresponding to the states of the particle. In contrast, when driving is strong, the detector returns a single response corresponding to the mean of the two single-state responses. This situation is similar to a motional averaging, observed in nuclear magnetic resonance spectroscopy. We study such quantum system, being periodically driven and probed, which consists of a qubit coupled to a quantum resonator. It is demonstrated that the transmission through the resonator is defined by the interplay between driving strength, qubit dissipation, and resonator linewidth. We demonstrate that our experimental results are in good agreement with numerical and analytical calculations.

1 Introduction

Circuit quantum electrodynamics studies scalable solid-state quantum systems, behaving analogous to the interacting light and matter, with superconducting qubits playing the role of artificial atoms. At this point, a number of quantum phenomena, known from atomic and optical physics, have been demonstrated in solid-state systems, such as lasing and cooling of the electromagnetic field in a resonator [1–6] and Mollow triplet [7–10]. Another phenomenon, called the *motional averaging* effect, which originated from nuclear magnetic resonance spectroscopy [11], has been also recently demonstrated with a superconducting qubit [12]. In that experiment, the qubit was driven by stochastic pulses. At the same time, a two tone spectroscopy was performed, which showed that the two spectroscopic lines (corresponding to two different states) are converted to a single broadened line for slow jumping rates, showing an increase of the average jumping rate [11, 12]. Different aspects of the motional averaging were studied recently, such as classical analogies [13], weighted averaging [14] and related studies (see Refs. [15,16]).

Reminiscent of motional averaging can be observed in a qubit-resonator system where, instead of a noisy signal, the qubit is driven by a periodic pump, with frequency $\omega_{\rm d}$ and amplitude Ω. The resonator which is dispersively coupled to the qubit, can be probed through its own driving term with frequency ω. The resulting transmission through the resonator exhibits two resonant lines for the weak qubit driving corresponding to the qubit states and a single line in between for when the qubit driving is increased, see Figure 1. This was demonstrated recently for a transmon-based system and termed *quantum rifling* [17] due to the lack of measurement back-action on the qubit from the driven resonator to the strongly driven qubit; see also references [18,19]. In this paper, we do not study measurement back-action but focus on the motional averaging picture for the resonator line and obtain simplified analytical expressions for resonator transmission.

Interaction of a quantum system with a quantized electromagnetic field is considered in the frame of the quantum Rabi model [20–26]. In the situation where the coupling strength g between the two-level system and the electromagnetic field is much smaller than the difference between the qubit $\omega_{\rm q}$ and resonator $\omega_{\rm r}$ frequencies, $|\omega_{\rm q} - \omega_{\rm r}| > {\rm g}$, this is known as the Jaynes-Cummings model [21,27–30].

* Contribution to the Topical Issue "Advances in Quasi-Periodic and Non-Commensurate Systems", edited by Tobias Stauber and Sigmund Kohler.

[a] e-mail: karpov@ilt.kharkov.ua

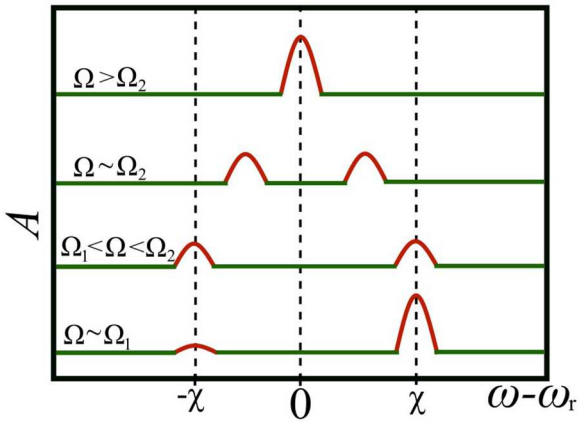

Fig. 1. Schematic of probabilistic motional averaging. If driven by a periodic signal, qubit's response (the resonator transmission amplitude A) is defined by the energy-level occupation probabilities. The height of the two peaks at $\Omega \sim \Omega_1$ is defined by the upper-level occupation probability and their position is defined by the dispersive shift χ. With increasing Ω, the two peaks, first, become of equal height and then merge into one, which we term as a probabilistic motional averaging. The characteristic frequency Ω_1 denotes when the upper-level occupation probability becomes significant and Ω_2 is in-between the two regimes: (i) when the peaks are at $\omega - \omega_\mathrm{r} = \pm\chi$ and (ii) when they merge into one, at $\omega = \omega_\mathrm{r}$.

Experiments are largely described by the semi-classical approximation, e.g. references [1,3,5,31–39], when a chain of equations is restrained by keeping only the first-order correlators. To describe time-evolution experiments, a semi-quantum approach is more correct [17,40,41]; comparison of the two approaches can be found e.g. in reference [42]. Note that in practice, to get a spectrum of a non-linear level structure of the system, one should apply two signals, to drive the system and a weak probe tone, which is known as a two-tone spectroscopy [38,43,44].

In this paper, we study measurement of a two-level system in the Rabi model, which is coupled to a coplanar-waveguide resonator as a cavity. The response of the system is calculated using the master equation for the density operator both numerically in the semi-quantum approximation and analytically in the semi-classical approximation. Varying the driving amplitude, we observe two different regimes, analogously to reference [17]: (i) weak-driving regime and (ii) strong-driving regime. In the first one, the weak-driving regime (i), both the ground and excited qubit states are monitored, displaying their probabilistic energy-level occupations. And when the power of driving is strong enough, in the strong-driving regime (ii), the spectral lines converge into a peak centered at the bare cavity and qubit transition frequencies. We note that the transition between these regimes can also be referred to as the driven quantum-to-classical transition [45–47].

2 Model

We study a two-level system which is coupled to a cavity. The system is driven by two signals: the high-amplitude driving tone with the frequency ω_d and the low-amplitude probe tone with the frequency ω. The qubit-resonator system we consider in the circuit-QED realization; specifically, it can be the driven transmon-resonator system [40,48–50], which is described by the Jaynes-Cummings Hamiltonian [20] in the two-level approximation:

$$H = \hbar\omega_\mathrm{r} a^\dagger a + \hbar\frac{\omega_\mathrm{q}}{2}\sigma_z + \hbar\mathrm{g}\left(\sigma_- a^\dagger + \sigma_+ a\right) + \hbar\xi\left(a^\dagger e^{-i\omega t} + a e^{i\omega t}\right) + \hbar\Omega\left(\sigma_+ e^{-i\omega_\mathrm{d} t} + \sigma_- e^{i\omega_\mathrm{d} t}\right). \quad (1)$$

Here, $\hbar\omega_\mathrm{q}$ is the transition energy between qubit states; σ_i and $\sigma_\pm = (\sigma_x \pm i\sigma_y)/2$ are Pauli operators; the resonator has the quantized fundamental mode with frequency ω_r; $a^\dagger(a)$ is the creation (annihilation) operator of a single excitation in the resonator; the coupling strength between the two-level system and the resonator is defined by $\hbar\mathrm{g}$; the probe and drive amplitudes are described by values ξ and Ω, respectively. Note that the transmon-resonator coupling constant g relates to the bare coupling g_0 as $\mathrm{g} = \mathrm{g}_0\sqrt{E_\mathrm{c}/|\Delta - E_\mathrm{c}|}$ with the detuning $\Delta = \hbar(\omega_\mathrm{q} - \omega_\mathrm{r})$ and the qubit charging energy E_c, where this renormalization is due to the virtual transitions through the upper transmon states. In the experiments, e.g. references [35,40,50], the measured value is the normalized transmission amplitude A. This is related to the photon field $\langle a\rangle$ in the cavity [40,50–52], $A = 2V_0|\langle a\rangle|$, where V_0 is a voltage related to the gain of the experimental amplification chain [50] and it is defined as [40] $V_0^2 = Z\hbar\omega_\mathrm{r}\varkappa/4$ with Z standing for the transmission-line impedance.

3 Semi-classical approach: analytical solution

To quantitatively describe the system, we first take the master equation in the form of equation (5) from reference [40]. This includes the resonator relaxation rate κ and qubit relaxation and pure dephasing rates, Γ_1 and $\Gamma_2 = \Gamma_\phi + \Gamma_1/2$. While the equations can be numerically solved in their available form, it is more illustrative to study analytical expressions first. For this purpose, we consider the steady-state solution in the so-called semi-classical approximation, where all correlators are assumed to factorize, $\langle a^\dagger\sigma\rangle \approx \langle a^\dagger\rangle\langle\sigma\rangle$, etc. [42] Then from the Lindblad equation, we obtain the non-linear equations for $\langle a\rangle$, $\langle\sigma\rangle$, and $\langle\sigma_z\rangle$. These can be rewritten for $n = |\langle a\rangle|^2$ and $\langle\sigma_z\rangle = 2P_+ - 1$, with P_+ standing for the qubit upper-level occupation probability, as follows

$$n = |\langle a\rangle|^2 = \frac{\xi^2}{\left[\chi(2P_+ - 1) + \delta\omega_\mathrm{r}\right]^2 + \kappa^2}, \quad (2)$$

$$P_+ = \frac{1}{2}\frac{\Omega^2}{\Omega^2 + \Omega_1^2(n)}, \quad (3)$$

$$\Omega_1^2(n) = \frac{4}{T_1 T_2} + 4\frac{T_2}{T_1}\left(\delta\omega_\mathrm{q} + 2\chi n\right)^2. \quad (4)$$

Here $\delta\omega_r = \omega_r - \omega$, $\delta\omega_q = \omega_q - \omega_d$, $\chi = g^2/\Delta$ describes the dispersive shift, and Ω_1 can be interpreted from equation (3), as the characteristic driving amplitude Ω, at which the excited qubit level becomes significantly occupied. In particular, at resonance ($\delta\omega_q = 0$) in the linear approximation (neglecting the term with n^2), we have the characteristic driving amplitude as in reference [50]: $\Omega_1 = 2\,(T_1T_2)^{-1/2}$. In general case, the characteristic driving amplitude Ω_1 depends on the measurement amplitude ξ and is defined by equation (4) together with equations (2) and (3).

4 Semi-quantum approach: numerical solution

The system Hamiltonian (1) can be rewritten in a more illustrative form for large detuning Δ between a transmon qubit (in the two-level approximation) and a resonator mode, $\Delta \equiv \hbar\,(\omega_q - \omega_r) \gg g$,

$$H' = \hbar(\delta\omega_r + \chi\sigma_z)a^\dagger a + \hbar\frac{\delta\omega_{q-d} + \chi}{2}\sigma_z + \hbar\xi(a^\dagger + a) + \hbar\frac{\Omega}{2}(\sigma + \sigma^\dagger), \quad (5)$$

where $\delta\omega_{q-d} = \omega_q - \omega_d$ and $\delta\omega_r = \omega_r - \omega$. It is reasonable to describe the system in the dispersive approximation of the Jaynes-Cummings Hamiltonian, as in references [40,49,53]. Then, following references [40–42], we obtain equations in the so-called semi-quantum model, where one assumes factoring of higher order terms and keeping only the second order correlators as the following: $\langle a^\dagger a\sigma_i\rangle \approx \langle a^\dagger a\rangle\langle\sigma_i\rangle$ and $\langle a^\dagger a a\sigma_i\rangle \approx \langle a^\dagger a\rangle\langle a\sigma_i\rangle$. This allows truncating the infinite series of equations. From the Lindblad equation, for the expectation values of the operators $\langle\sigma_i\rangle$ $(i = x, y, z)$ and the resonator field operators $\langle a\rangle$, $\langle a\sigma_i\rangle$, and $\langle a^\dagger a\rangle$ we obtain the system of equations, known as the Maxwell-Bloch equations:

$$\frac{d}{dt}\langle\sigma_z\rangle = \Omega\langle\sigma_y\rangle - \Gamma_1\left(1 + \frac{\langle\sigma_z\rangle}{z_0}\right), \quad (6a)$$

$$\frac{d}{dt}\langle\sigma_x\rangle = -\left(2\chi\langle a^\dagger a\rangle + \delta\omega_{q-d} + \chi\right)\langle\sigma_y\rangle - \Gamma_2\frac{\langle\sigma_x\rangle}{z_0}, \quad (6b)$$

$$\frac{d}{dt}\langle\sigma_y\rangle = \left(2\chi\,\langle a^\dagger a\rangle + \delta\omega_{q-d} + \chi\right)\langle\sigma_x\rangle - \Gamma_2\frac{\langle\sigma_y\rangle}{z_0} - \Omega\langle\sigma_z\rangle, \quad (6c)$$

$$\frac{d}{dt}\langle a\rangle = -i\left(\delta\omega_r\langle a\rangle + \chi\langle a\sigma_z\rangle + \xi\right) - \kappa\langle a\rangle, \quad (6d)$$

$$\frac{d}{dt}\langle a^\dagger a\rangle = -2\xi\,\mathrm{Im}\,\langle a\rangle + 2\kappa\left(N_{th} - \langle a^\dagger a\rangle\right), \quad (6e)$$

$$\frac{d}{dt}\langle a\sigma_z\rangle = -i\left(\delta\omega_r\,\langle a\sigma_z\rangle + \chi\langle a\rangle + \xi\langle\sigma_z\rangle\right) + \Omega\langle a\sigma_y\rangle - \Gamma_1\,\langle a\rangle - \left(\frac{\Gamma_1}{z_0} + \kappa\right)\langle a\sigma_z\rangle, \quad (6f)$$

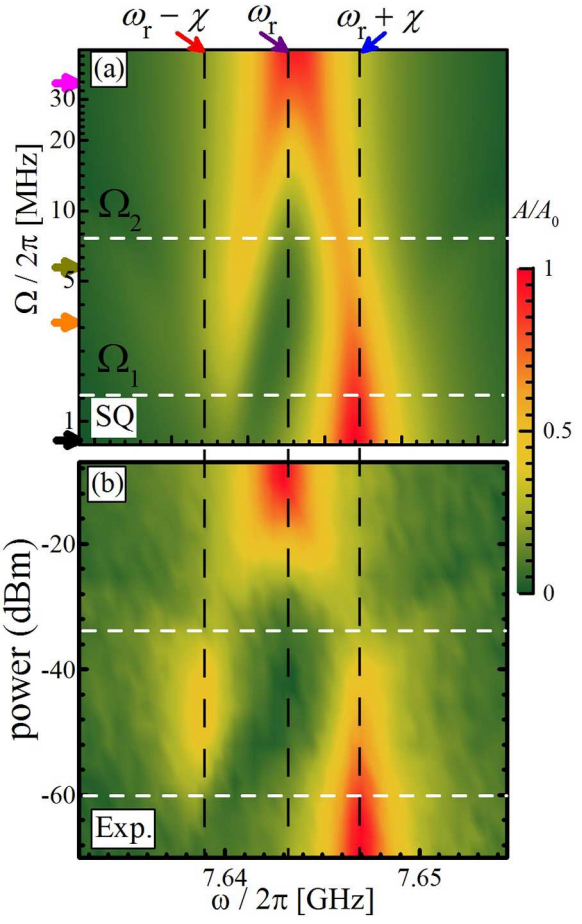

Fig. 2. Regimes for the driven and probed qubit and characteristic driving amplitudes Ω_1 and Ω_2. (a) Normalized transmission amplitude A as a function of the probe frequency ω and driving amplitude Ω. The picture is a result of the steady-state solution of Maxwell-Bloch equations (6). Horizontal colour arrows show position of the cuts, presented in the next figure. (b) Respective experimental measurement.

$$\frac{d}{dt}\langle a\sigma_x\rangle = -i\delta\omega_r\,\langle a\sigma_x\rangle - \left(\frac{\Gamma_2}{z_0} + \kappa\right)\langle a\sigma_x\rangle - \left(\delta\omega_{q-d} + 2\chi\left(\langle a^\dagger a\rangle + 1\right)\right)\langle a\sigma_y\rangle - i\xi\langle\sigma_x\rangle, \quad (6g)$$

$$\frac{d}{dt}\langle a\sigma_y\rangle = -i\delta\omega_r\,\langle a\sigma_y\rangle - \left(\frac{\Gamma_2}{z_0} + \kappa\right)\langle a\sigma_y\rangle - i\xi\langle\sigma_y\rangle - \Omega\langle a\sigma_z\rangle + \left(\delta\omega_{q-d} + 2\chi\left(\langle a^\dagger a\rangle + 1\right)\right)\langle a\sigma_x\rangle. \quad (6h)$$

We have numerically solved the system of equations (6) and the results are presented in Figures 2–4, where the normalized transmission amplitude is plotted as a function of the driving power and probing frequency. For calculations we take the following parameters, close to the ones of reference [17]:

$$\frac{\omega_r}{2\pi} = 7.643\ \text{GHz}, \quad \frac{\omega_q}{2\pi} = 6.440\ \text{GHz}, \quad \frac{\chi}{2\pi} = 4.1\ \text{MHz}, \quad T_1 = 1.55\ \mu\text{s}, \quad T_2 = 2.65\ \mu\text{s}, \quad \kappa/2\pi = 1\ \text{MHz}. \quad (7)$$

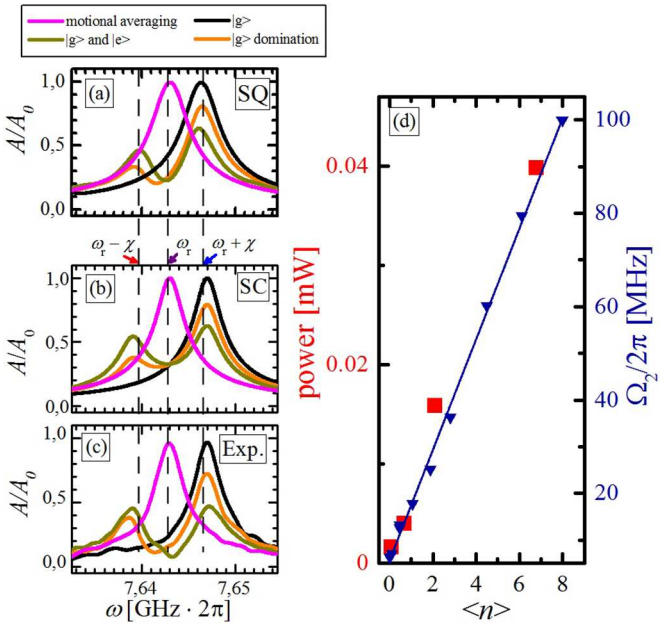

Fig. 3. Shift of the resonance lines. Numerical semi-quantum (a) and analytical semi-classical (b) dependencies of the normalized transmission amplitude A on the probing frequency for several values of driving power Ω, shown by the arrows in Figure 2. Solid lines relate to regime (i) with two qubit lines and the dashed lines are for the regime (ii) with one motional-averaged line. (c) Respective experimental measurement. (d) Characteristic driving amplitude Ω_2 as a function of the photon number $\langle n\rangle$; right scale is for the theoretical points (Ω_2 in MHz) and left scale is for the experimental points (power in mW); the agreement between the data here could be used for the calibration of the power.

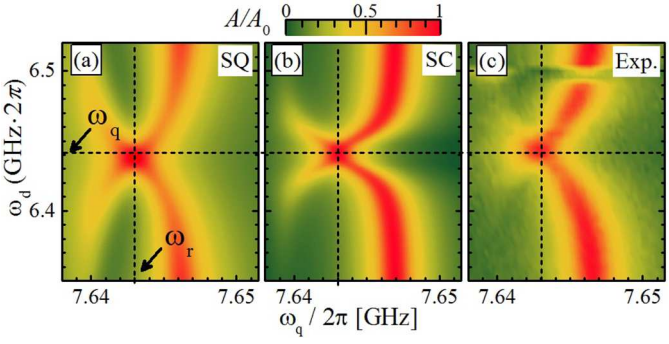

Fig. 4. The resonant transmission shift. Analytical (a) and semi-quantum (b) dependencies of the normalized transmission amplitude A on the probe frequency ω and the drive frequency ω_d. (c) Respective experimental measurement.

5 Experiment

Our sample consists of a transmon qubit (named Qubit 2 in Ref. [17]) with a transition frequency between its ground and first excited states $\omega_q/(2\pi) = 6.44$ GHz coupled to a superconducting co-planar waveguide resonator with resonance frequency $\omega_r/(2\pi) = 7.643$ GHz. The qubit state can be controlled by applying a coherent drive tone with frequency $\omega_d \simeq \omega_q$ through a separate charge line. The interaction between the qubit and the resonator results in a shift of the resonator frequency dependent on the qubit state. This dispersive shift of $\chi/(2\pi) = 4.1$ MHz allows us to perform the read out of the qubit state by applying a probe tone to the resonator at frequency $\omega_p \simeq \omega_r$ and by subsequent detection of the transmitted signal with a standard heterodyne detection scheme (see Ref. [17]).

6 Results

Numerical and analytical results of the previous two sections together with the experimental observations are presented in Figures 2–4. Namely, in Figure 2a we plot the transmission amplitude A, normalized to its maximal value A_0, as a function of the probe frequency ω and driving amplitude Ω, which is calculated using the equations and parameters from the previous section, equations (6)-(7). Several horizontal cuts of Figure 2a are presented as Figures 2a–2c, which is the transmission plotted as a function of the probe frequency ω for several values of the drive amplitude Ω (see explanations below).

In Figure 2a we can observe two different regimes. Let us now analyze these regimes in more detail, since these present the main result of our work here.

(i) $\Omega \ll \Omega_2$. This can be called the "fast-measurements" regime, or equivalently weak-driving regime, or "quantum" regime. This is because the two qubit states are visualized with the position of the respective resonances at $\delta\omega = \pm\chi$. So, in this regime both ground and excited qubit states are monitored, with respective probabilities. Namely, with increasing the driving amplitude Ω, the probability of finding the qubit in the excited state increases, left line in Figure 2a, while the probability of the ground state (right resonance line) decreases. See also about this, e.g., in reference [54].

(ii) $\Omega \gg \Omega_2$. This can be called the "slow-measurements" regime, or equivalently strong-driving regime, or "classical" regime. This corresponds to no frequency shift, with qubit states equally populated, which thus can also be referred to as a "motional averaging". Similar transitions from a "quantum" to "classical" regime was observed in references [12,17,45,46,55].

Figure 3d shows the dependence of the characteristic driving amplitude Ω_2, which separates regimes (i) and (ii), as a function of photon numbers obtained from our numerical solution as well as the experimental points. The theoretical points were calculated for the probe amplitudes ξ from 0.01κ to 2κ. The experimental points were taken from Fig. S4 of reference [17].

Let us now consider interpretation of the above results analytically, for the two respective regimes.

Regime (i). This is not described directly by the stationary solution. To describe this regime we note that in this case the qubit is found either in the ground state with

the probability P_- or in the excited state with the probability P_+. Then the measured normalized transmission amplitude can be calculated as following

$$A = P_- A_- + P_+ A_+ \tag{8}$$

with the partial values $A_\pm$ given by equation (2):

$$A_\pm = \frac{\xi}{\sqrt{\left[\pm\chi + \delta\omega_\mathrm{r}\right]^2 + \kappa^2}}. \tag{9}$$

With these formulas we plot the solid lines in Figure 3b.

Regime (ii). Under the strong resonant driving, the qubit levels are equally populated and then equation (2) with $P_+ = 1/2$ yields

$$A = \frac{\xi}{\sqrt{\delta\omega_\mathrm{r}^2 + \kappa^2}}. \tag{10}$$

With this formula we plot the magenta solid line in Figure 3a.

Finally we describe both the qubit and resonator frequency shifts. For this, we make use of equation (8) with the partial transmission amplitudes $A_\pm$ defined by the respective probabilities, rather than assuming them equal to 0 or 1 as in equation (9), as following

$$A_\pm = \frac{\xi}{\sqrt{\left[\chi\left(1 - 2P_\pm\right) + \delta\omega_\mathrm{r}\right]^2 + \kappa^2}}. \tag{11}$$

With this analytical formulas we plot Figure 4b, which is remarkably in agreement with the numerical result in Figure 4a and the experiment in Figure 4c.

Note that the advantage of the analytical results, presented here, is that these are transparent formulas, which capture the main physics here. Importantly, these results are confirmed by the numerical calculations, done within the semi-quantum model, and by comparison with the experiments.

7 Conclusions

We have studied the interaction between a cavity and a two-level system in the Jaynes-Cummings model with dispersive coupling under external drive. We have demonstrated that there are two different regimes. The quantum and semi-classical regimes demonstrate detection of the two energy transitions in the system, while at higher driving amplitude the two resonance lines merge into one, making a specific motional-averaging picture, defined by the qubit energy-level occupation probabilities. We believe that our analytical and numerical results are useful for deeper understanding of both experimental realizations and theoretical description of dynamical phenomena in circuit quantum electrodynamics.

D.S.K. is grateful to A. Sultanov for fruitful discussions. D.S.K. acknowledges the hospitality of the Leibniz Institute of Photonic Technology, where part of this work was done. The work of D.S.K. was partly supported by DAAD Binationally Supervised Doctoral Degrees Research Grant (No. 57299293) and DAAD Short-Term Research Grant (No. 57381332). S.N.S. and D.S.K. acknowledge partial support by the Grant of the President of Ukraine (Grant No. F84/185-2019). D.S., A.G.F. and A.F. were supported by the Australian Research Council Centre of Excellence for Engineered Quantum Systems (EQUS, CE170100009).

Author contribution statement

All the authors were involved in the preparation of the manuscript. All the authors have read and approved the final manuscript.

References

1. O. Astafiev, K. Inomata, A.O. Niskanen, T. Yamamoto, Y.A. Pashkin, Y. Nakamura, J.S. Tsai, Nature **449**, 588 (2007)
2. S. Ashhab, J.R. Johansson, A.M. Zagoskin, F. Nori, New J. Phys. **11**, 023030 (2009)
3. M. Grajcar, S.H.W. van der Ploeg, A. Izmalkov, E. Il'ichev, H.G. Meyer, A. Fedorov, A. Shnirman, G. Schön, Nature Phys. **4**, 612 (2008)
4. F. Nori, Nature Phys. **4**, 589 (2008)
5. J. Hauss, A. Fedorov, S. André, V. Brosco, C. Hutter, R. Kothari, S. Yeshwanth, A. Shnirman, G. Schön, New J. Phys. **10**, 095018 (2008)
6. J.Q. You, Y.x. Liu, F. Nori, Phys. Rev. Lett. **100**, 047001 (2008)
7. L. Zhou, Z.R. Gong, Y.x. Liu, C.P. Sun, F. Nori, Phys. Rev. Lett. **101**, 100501 (2008)
8. O. Astafiev, A.M. Zagoskin, A.A. Abdumalikov, Y.A. Pashkin, T. Yamamoto, K. Inomata, Y. Nakamura, J.S. Tsai, Science **327**, 840 (2010)
9. Y.S. Greenberg, A.N. Sultanov, Phys. Rev. A **95**, 053840 (2017)
10. A.A. Abdumalikov, O.V. Astafiev, Y.A. Pashkin, Y. Nakamura, J.S. Tsai, Phys. Rev. Lett. **107**, 043604 (2011)
11. A. Abragam, *Principles of Nuclear Magnetism* (Oxford, Oxford University Press, 1986)
12. J. Li, M.P. Silveri, K.S. Kumar, J.M. Pirkkalainen, A. Vepsäläinen, W.C. Chien, J. Tuorila, M.A. Sillanpää, P.J. Hakonen, E.V. Thuneberg et al., Nat. Commun. **4**, 1420 (2013)
13. O.V. Ivakhnenko, S.N. Shevchenko, F. Nori, Sci. Rep. **8**, 12218 (2018)
14. K. Ono, S.N. Shevchenko, T. Mori, S. Moriyama, F. Nori, Phys. Rev. Lett. **122**, 207703 (2019)
15. S. Kono, Y. Masuyama, T. Ishikawa, Y. Tabuchi, R. Yamazaki, K. Usami, K. Koshino, Y. Nakamura, Phys. Rev. Lett. **119**, 023602 (2017)
16. J. Pan, Y. Fan, Y. Li, X. Dai, X. Wei, Y. Lu, C. Cao, L. Kang, W. Xu, J. Chen et al., Phys. Rev. B **96**, 024502 (2017)
17. D. Szombati, A.G. Frieiro, C. Müller, T. Jones, M. Jerger, A. Fedorov, Phys. Rev. Lett. **124**, 070401 (2020)
18. S. Ashhab, J.Q. You, F. Nori, New J. Phys. **11**, 083017 (2009)
19. S. Ashhab, J.Q. You, F. Nori, Phys. Scr. **T137**, 014005 (2009)

20. W.P. Schleich, *Quantum Optics in Phase Space* (Wiley-VCH, Berlin, 2001)
21. M.O. Scully, M.S. Zubairy, *Quantum Optics* (Cambridge, Cambridge University Press, 1997)
22. X. Gu, A.F. Kockum, A. Miranowicz, Y. Xi Liu, F. Nori, Phys. Rep. **718–719**, 1 (2017)
23. A.F. Kockum, F. Nori, in *Quantum Bits with Josephson Junctions* (Springer International Publishing, 2019), p. 703
24. J.M. Pirkkalainen, S.U. Cho, F. Massel, J. Tuorila, T.T. Heikkila, P.J. Hakonen, M.A. Sillanpää, Nat. Commun. **6**, 6981 (2014)
25. M. Silveri, J. Tuorila, M. Kemppainen, E. Thuneberg, Phys. Rev. B **87**, 134505 (2013)
26. A.P. Saiko, R. Fedaruk, A. Kolasa, S.A. Markevich, Phys. Scr. **85**, 045301 (2012)
27. A.M. Zagoskin, *Quantum Engineering: Theory and Design of Quantum Coherent Structures* (Cambridge University Press, 2011)
28. G. Wendin, Rep. Prog. Phys. **80**, 106001 (2017)
29. S.N. Shevchenko, *Mesoscopic Physics meets Quantum Engineering* (World Scientific, Singapore, 2019)
30. A.P. Saiko, R. Fedaruk, S.A. Markevich, J. Phys. B: At. Mol. Opt. Phys. **47**, 9 (2014)
31. J.Q. You, Y.X. Liu, C.P. Sun, F. Nori, Phys. Rev. B **75**, 104516 (2007)
32. P. Scarlino, D.J. van Woerkom, U.C. Mendes, J.V. Koski, A.J. Landig, C.K. Andersen, S. Gasparinetti, C. Reichl, W. Wegscheider, K. Ensslin et al., Nat. Commun. **10**, 3011 (2018)
33. M. Silveri, K. Kumar, J. Tuorila, J. Li, A. Vepsäläinen, E. Thuneberg, G. Paraoanu, New J. Phys. **17**, 043058 (2015)
34. H. Ian, Y.x. Liu, F. Nori, Phys. Rev. A **81**, 063823 (2010)
35. G. Oelsner, P. Macha, O.V. Astafiev, E. Il'ichev, M. Grajcar, U. Hübner, B.I. Ivanov, P. Neilinger, H.G. Meyer, Phys. Rev. Lett. **110**, 053602 (2013)
36. S.N. Shevchenko, G. Oelsner, Y.S. Greenberg, P. Macha, D.S. Karpov, M. Grajcar, U. Hübner, A.N. Omelyanchouk, E. Il'ichev, Phys. Rev. B **89**, 184504 (2014)
37. D.S. Karpov, G. Oelsner, S.N. Shevchenko, Y.S. Greenberg, E. Ilichev, Low Temp. Phys. **42**, 189 (2016)
38. G. Oelsner, E. Il'ichev, U. Hübner, Phys. Rev. B **101**, 054511 (2020)
39. Y.H. Chang, D. Dubyna, W.C. Chien, C.H. Chen, C.S. Wu, W. Kuo, arXiv:1906.06730 (2019)
40. R. Bianchetti, S. Filipp, M. Baur, J.M. Fink, M. Göppl, P.J. Leek, L. Steffen, A. Blais, A. Wallraff, Phys. Rev. A **80**, 043840 (2009)
41. S. André, V. Brosco, M. Marthaler, A. Shnirman, G. Schön, Phys. Scr. **137**, 014016 (2009)
42. S.N. Shevchenko, D.S. Karpov, Phys. Rev. Appl. **10**, 014013 (2018)
43. A.P. Saiko, S.A. Markevich, R. Fedaruk, Phys. Rev. A **93**, 063834 (2016)
44. S. Kohler, Phys. Rev. A **98**, 023849 (2018)
45. I. Pietikäinen, S. Danilin, K.S. Kumar, J. Tuorila, G.S. Paraoanu, J. Low Temp. Phys. **191**, 354 (2018)
46. I. Pietikäinen, S. Danilin, K.S. Kumar, A. Vepsäläinen, D.S. Golubev, J. Tuorila, G.S. Paraoanu, Phys. Rev. B **96**, 020501 (2017)
47. I. Pietikäinen, J. Tuorila, D.S. Golubev, G.S. Paraoanu, Phys. Rev. A **99**, 063828 (2019)
48. J.Q. You, X. Hu, S. Ashhab, F. Nori, Phys. Rev. B **75**, 140515 (2007)
49. J. Koch, T.M. Yu, J. Gambetta, A.A. Houck, D.I. Schuster, J. Majer, A. Blais, M.H. Devoret, S.M. Girvin, R.J. Schoelkopf, Phys. Rev. A **76**, 042319 (2007)
50. L.S. Bishop, J.M. Chow, J. Koch, A.A. Houck, M.H. Devoret, E. Thuneberg, S.M. Girvin, R.J. Schoelkopf, Nat. Phys. **5**, 105 (2009)
51. P. Macha, G. Oelsner, J.M. Reiner, M. Marthaler, S. André, G. Schön, U. Hübner, H.G. Meyer, E. Il'ichev, A.V. Ustinov, Nat. Commun. **5**, 5146 (2014)
52. A.L. Rakhmanov, A.M. Zagoskin, S. Savel'ev, F. Nori, Phys. Rev. B **77**, 144507 (2008)
53. G. Oelsner, S.H.W. van der Ploeg, P. Macha, U. Hübner, D. Born, S. Anders, E. Il'ichev, H.G. Meyer, M. Grajcar, S. Wünsch et al., Phys. Rev. B **81**, 172505 (2010)
54. M. Reagor, W. Pfaff, C. Axline, R.W. Heeres, N. Ofek, K. Sliwa, E. Holland, C. Wang, J. Blumoff, K. Chou et al., Phys. Rev. B **94**, 014506 (2016)
55. J.M. Fink, L. Steffen, P. Studer, L.S. Bishop, M. Baur, R. Bianchetti, D. Bozyigit, C. Lang, S. Filipp, P.J. Leek et al., Phys. Rev. Lett. **105**, 163601 (2010)